Parametrization of 1-Butyl-3-methylimidazolium Hexafluorophosphate/Nitrate Ionic Liquid for the GROMOS Force Field

Nuno M. Micaelo, António M. Baptista, and Cláudio M. Soares*

Instituto de Tecnologia Química e Biológica, Universidade Nova de Lisboa, Av. da República, Apartado 127, 2781-901 Oeiras, Portugal

Received: March 26, 2006; In Final Form: May 25, 2006

A united-atom model of 1-butyl-3-methylimidazolium hexafluorophosphate ([BMIM][PF_6]) and 1-butyl-3-methylimidazolium nitrate ([BMIM][NO_3]) is developed in the framework of the GROMOS96 43A1[1] force field. These two ionic liquids are parametrized, and their equilibrium properties in the 298−363 K temperature range are subjected to validation against known experimental properties, namely, density, self-diffusion, shear viscosity, and isothermal compressibility. The ionic radial/spatial distributions, π interaction, gauche/trans populations of the butyl tail, and enthalpies of vaporization are also reported. The properties obtained from the molecular dynamics simulations agree with experimental data and have the same temperature dependence. The strengths and weakness of our model are discussed.

Introduction

Several room-temperature ionic liquids (RTILs) have been parametrized recently in the framework of current biomolecular force fields (FFs) such as AMBER,[2] OPLS,[3] and CHARMM.[4] These molecular models are all-atom descriptions of the RTIL molecules under study and, with the exception of the models presented by Hanke et al.,[5] Shah et al.,[6] and recently by Liu et al.,[7] there is no united-atom parametrization of a RTIL suitable to be employed in the context of the GROMOS96 43A1 FF.[1] RTILs are a new class of organic salts that have drawn great attention from researchers because of their molecular properties as solvents in catalytic applications. For a recent review of RTIL properties see Wilkes,[8] and for their applications see Dupont et al.,[9] Olivier-Bourbigou, and Magna.[10] The parametrization of a new set of molecules demands its validation against experimental data. Although there are still few reports on the structural and thermodynamic properties of RTILs in general, there is a considerable amount of other experimental data for [BMIM][PF_6], such as self-diffusion,[11−13] viscosity,[11,14−19] density,[11,15,19−22] and isothermal compressibility.[20] The validation can also be supported qualitatively by data from studies of similar RTILs using NMR,[23,24] probe-based fluorescence spectroscopy,[25−27] neutron diffraction,[28] quasielastic neutron scattering,[29] X-ray diffraction,[30] and ab initio calculations.[31] [BMIM][PF_6] has been studied by several groups using molecular mechanics/dynamics (MM/MD) methods[5,32−37] in order to reproduce experimental data and provide a molecular description of this type of system.

The present work provides a parametrization of two RTILs, [BMIM][PF_6] and [BMIM][NO_3], in the context of the GROMOS96 43A1 FF.[1] The models are built and validated using known experimental data on dynamic and structural properties. Additional properties of the RTIL liquid phase are also provided, such as enthalpy of vaporization and radial/spatial distribution functions, even though no experimental data is yet available for comparison. The RTIL models will be applied to our research on biocatalysis in nonaqueous media and provide the groundwork for further parametrization of other imidazole-based RTILs.

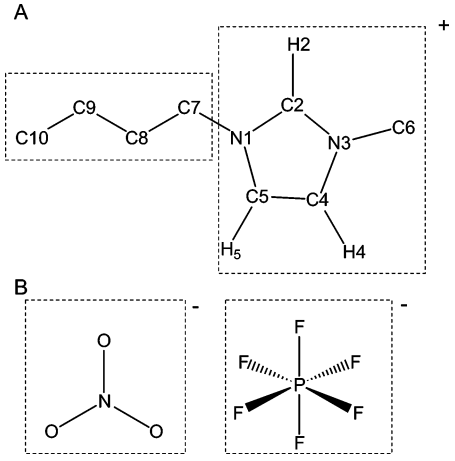

Figure 1. Schematic representation of (A) $[BMIM]^+$ and (B) $[PF_6]^-$ and $[NO_3]^-$ united atom molecular topology based on the GROMOS FF. Atom types are described in Table 1. Charge groups are enclosed by dashed lines.

Methodology

Force-Field Parameters. A united-atom model was built for [BMIM][PF_6] and [BMIM][NO_3] (Figure 1). The cation $[BMIM]^+$ is modeled using a united-atom description for the CH_2 and CH_3 groups of the butyl tail (C10−C9−C8−C7) and for the methyl group (C6) attached to the imidazole ring (Figure 1A). The imidazole ring is based on the histidine building block available in the GROMOS96 43A1 FF[1] and takes into account the presence of explicit aromatic hydrogen atoms in the ring. The inclusion of these hydrogen atoms was due to their marked polar character, as evidenced by our partial charge calculations (see below) and also from other ab initio[31] and experimental[23,24,30] evidences of their role in hydrogen bonding with the anion species. Furthermore, in the recent parametrization of the

* Corresponding author. Tel: +351 21 4469610. Fax: +351 21 4433644. E-mail: claudio@itqb.unl.pt.

10.1021/jp061869s CCC: $33.50
Published on Web 06/30/2006

TABLE 1: Atom Types and Partial Atom Charges of $[BMIM]^+$, $[PF_6]^-$, and $[NO_3]^-$ [a]

ion	name	43A1 atom type	charge
$[BMIM]^+$	N1	NR	−0.103
	C2	C	−0.104
	H2	HC	0.262
	N3	NR	0.039
	C6	CH3	0.323
	C4	C	−0.152
	H4	HC	0.232
	C5	C	−0.159
	H5	HC	0.242
	C7	CH2	0.320
	C8	CH2	0.099
	C9	CH2	0.000
	C10	CH3	0.000
$[PF_6]^-$	P	PIL[b]	1.101
	F	FIL[b]	−0.350
$[NO_3]^-$	N	NIL[b]	1.088
	O	OIL[b]	−0.696

[a] Atom types and partial atom charges of $[BMIM]^+$, $[PF_6]^-$, and $[NO_3]^-$. Atom types for the cation are taken from the GROMOS96 43A1 FF.[1] [b] Anion atom types developed in this study (see Table 2 for vdW parameters). See Figure 1 for the atom name correspondence.

GROMOS FF 53A5/53A6,[38] the histidine building block was rebuilt in order to include aromatic hydrogen atoms, similar to what was done previously for other aromatic groups. For the cation, bonded and nonbonded (Table 1) terms were derived from similar building blocks present in the GROMOS96 43A1 FF,[1] such as the histidine imidazole ring and aliphatic chains. Geometry optimization of the all-atom model of $[BMIM]^+$ was performed in the gas phase at the Hartree−Fock level, using the 6-31G(d) basis set. Partial atom charges were obtained using the RESP method[39] using a single step, based on electrostatic potentials calculated with the 6-31G(d) basis set by GAUSSIAN98[40] (Table 1). The only hydrogen atoms modeled in RESP were the ones attached to the ring heavy atoms. The last two carbon atoms of the tail (C9 and C10 in Figure 1) were forced to have zero charge, following the GROMOS practice. Nevertheless, in unrestrained calculations (data not shown) these atoms displayed charges close to zero. Forcing carbon C8 to have zero charge yielded a quite large charge on carbon C7, so it was decided to allow atom C8 to have charge. Charge groups were defined as depicted in Figure 1A. Quite recently, similar partial charge calculations were published for the same cation model by Liu et al.[7] These partial charges are overall similar to the ones reported here, with some localized differences, possibly due to the use of the 6-31G+(d) basis set, to the fact that no carbon atom was forced to have zero charge, and the two-step RESP approach employed by the authors.

The anion species $[PF_6]^-$ and $[NO_3]^-$ are not present in the current GROMOS FF.[41] However, several parametrizations can be found for these molecules in the literature.[5,32,33,35−37] Geometry optimization and partial charges for the anions (Table 1) were calculated in the same way as described previously for the cation. Bond distances were constrained to the values obtained by geometry optimization, and angles were set to obey to the known geometry of these molecules, planar for the $[NO_3]^-$ anion and an octahedral shape for $[PF_6]^-$. The refinement of the [BMIM][PF_6] and [BMIM][NO_3] models was made by varying the σ and ϵ van der Waals (vdW) parameters until an optimized model was obtained (Table 2), as judged from the comparison with the experimental data of viscosity, self-diffusion coefficient and density for these liquids. These properties were sensitive to the ϵ and σ assigned to the F and O atoms of $[PF_6]^-$ and $[NO_3]^-$, respectively. Low ϵ values were assigned to P and N atoms because they are shielded by the surrounding covalently bound F and O atoms, in an approach similar to that done by Hanke[5] using Buckingham potentials. Density was optimized by changing σ. Self-diffusion increased and shear viscosity decreased as we reduced ϵ assigned to the F and O atoms. The vdW interactions for different atom types were calculated using the geometric combination rule. In the 43A1 FF, there are up to three types of C12 interactions: type I is of general use, type II for atoms involved in hydrogen bonds, and type III for charged groups, like ions. In our model, we only take into consideration C12 type I interactions derived from σ and ϵ parameters.

TABLE 2: $[PF_6]^-$ and $[NO_3]^-$ vdW Parameters[a]

atom	ϵ (kJ/mol)	σ (nm)
PIL	0.0010	0.3370
FIL	0.1900	0.2946
NIL	0.0100	0.3150
OIL	0.1500	0.3037

[a] vdW parameters for the atoms of $[PF_6]^-$ and $[NO_3]^-$ anions developed in this study. Interactions between unlike atom types were calculated using the geometric combination rule.

System Setup. The solid state of some RTILs has been characterized by X-ray diffraction studies,[30,42−44] and their liquid phase has been characterized by NMR[23,24,45] and neutron diffraction[28] studies. Several authors suggest that the liquid phase of RTILs resembles the solid-state structure.[43,46,47] According to a model proposed by Dupont,[47] RTILs could be described as a supramolecular hydrogen-bonded polymeric structure, with a general pattern in the solid phase that is maintained in the liquid phase. Relaxation events probed by neutron scattering for this type of liquid have been measured in the subnanosecond time scale, suggesting that slower dynamics events exist in the system.[29] Viscosity measurements of several ionic liquids such as those employed in this study give very high values.[23,24,45]

In setting up a starting molecular configuration for MM/MD simulations of this type of system, care must be taken in order to avoid the possibility of simulating a system trapped in local minima due to an initially imposed artificial ion ordering. Thus, we tried to avoid bottlenecks of this type by a random displacement of cations and anions in a cubic box and by performing relatively long simulations for this type of system. The liquid state of [BMIM][PF_6] and [BMIM][NO_3] was simulated by building a initial molecular system comprised of 210 cations and 210 anions, with their position and orientation randomly assigned in a cubic box. The initial configuration consisting of atom positions and box vectors were rescaled in order to start the simulations of each RTIL at the known density at 363.15 K.

Simulation Details. The systems were simulated at selected temperatures: 298.15, 303.15, 313.15, 323.15, 333.15, 343.15, 353.15, and 363.15 K, a temperature range for which experimental data on density, viscosity, and self-diffusion properties are available (Tables 3 and 4).

MD/MM simulations were performed with the GROMACS[48,49] package. Bond lengths were constrained with LINCS.[50] Nonbonded interactions were calculated explicitly up to 9 Å and long-range electrostatic interactions were treated with PME[51,52] with a grid spacing of 1.2 Å and a fourth-order interpolation. Neighbor searching was done up to 9 Å and updated every five steps. A time step of integration of 2 fs was used. Initial configurations for both [BMIM][PF_6] and [BMIM]-

TABLE 3: Experimental and Simulation Properties of [BMIM][PF_6][a]

							self-diffusion coefficient (10^{-8} cm^2/s)			
	density (g/cm^3)			viscosity (cP)			cation		anion	
temp (K)	sim	ref 10	ref 14	sim	ref 10	ref 14	sim	ref 10	sim	ref 10
293.15		1.3753	1.3727		369.7	371		5.3		3.8
298.15	1.3576 (0.0024)	1.3709		245.9 (37.1)	258.7		5 (3)	7.2	2 (1)	5.2
303.15	1.3530 (0.0021)	1.3666	1.3626	181.8 (23.7)	187.5	204	11 (3)	9.6	5 (1)	7.0
313.15	1.3465 (0.0060)	1.3579	1.3565	102.6 (10.8)	107.3	125	12 (9)	15.9	6 (2)	12.0
323.15	1.3343 (0.0021)		1.3473	61.8 (5.5)	67.3	82.0	22 (2)	24.9	12 (0)	19.0
333.15	1.3257 (0.0030)		1.3359	41.5 (3.3)	45.3	55.1	30 (4)	36.7	18 (3)	28.5
343.15	1.3153 (0.0017)		1.3285	33.3 (2.4)	32.3	37.8	46 (0)	51.8	26 (7)	41.0
353.15	1.3042 (0.0026)		1.3225	24.5 (1.5)	24.0	25.3	67 (3)	70.5	47 (3)	56.6
363.15	1.2966 (0.0018)		1.3126	13.7 (1.1)		19.5	75 (19)	93.0	50 (0)	75.8

[a] See the text for details of the calculated properties calculations. Errors from simulations are calculated using the following: block averaging for density; eq 25 from Hess[56] for viscosity; and the difference of the self-diffusion coefficients obtained from fits over the two halves of the fit interval for the self-diffusion coefficient. See Figures 2−4 for plotted data.

TABLE 4: Experimental and Simulation Properties of [BMIM][NO_3][a]

					self-diffusion coefficient (10^{-8} cm^2/s)	
	density (g/cm^3)		viscosity (cP)		cation	anion
temp (K)	sim	ref 14	sim	ref 14	sim	sim
293.15		1.1574		266		
298.15	1.1603 (0.0016)		177.0 (33.6)		5 (4)	3 (3)
303.15	1.1545 (0.0023)	1.1497	135.4 (22.3)	144	7 (3)	5 (2)
313.15	1.1499 (0.0018)	1.1435	63.3 (7.2)	85.0	10 (1)	7 (2)
323.15	1.1416 (0.0016)	1.1372	60.5 (6.7)	54.1	20 (8)	19 (1)
333.15	1.1328 (0.0012)	1.1309	33.8 (3.4)	36.9	28 (6)	24 (2)
343.15	1.1263 (0.0012)	1.1239	23.0 (1.9)	25.9	42 (2)	45 (5)
353.15	1.1190(0.0014)	1.1167	19.5 (1.5)	18.9	64 (3)	61 (2)
363.15	1.1124 (0.0017)	1.1120	13.4 (0.9)	14.6	83 (8)	80 (6)

[a] See the text for details of the calculated properties calculations and legend of Table 2 for error calculations. See Figures 2 and 3 for plotted data.

$[NO_3]$ were energy minimized for 5000 steps using the steepest descent method, to remove bad contacts resulting from the initial random configuration of cations and anions. The simulations were initialized in the canonical ensemble during 100 ps for an initial equilibration at the different temperatures under study (Tables 3 and 4). The equilibration phase was continued for 5 ns in the isothermal−isobaric ensemble to ensure the full equilibration of all system properties. Additional 5-ns simulations in the isothermal−isobaric ensemble were used for data collection and analysis. The pressure control was implemented using the Berendsen barostat[53] with a reference pressure of 1 atm, a relaxation time of 1.0 ps, and an isothermal compressibility of 4.5×10^{-5} bar^{-1}. Temperature control was set using the Berendsen thermostat.[53] Cations and anions were separated in two heat baths with temperature coupling constants of 0.1 ps.

Shear viscosity calculations were performed employing the periodic perturbation method;[54,55] This method and others have been reviewed in a recent work by Hess.[56] Because improved accuracy can be obtained by increasing the system size, a new box was built by replicating previously equilibrated systems along the *z* axis, resulting in a final box with an approximate final size of $4 \times 4 \times 12$ nm, containing 630 cations and 630 anions. The external periodic acceleration profile for each particle was set to 0.01 nm ps^{-2}, and the heat generated by the viscous friction was removed by coupling to a heat bath. The systems were simulated at the selected temperatures (Tables 3 and 4) and equilibrated for 1−3 ns. At lower temperatures the cations and anions in liquid phase have lower rotational correlation times,[24] and thus longer times are need for equilibration at low temperatures. Shear viscosity was calculated from a 3-ns-length simulation after equilibration.

Results and Discussion

vdW Parameter Development. The optimization of our model relies on the parametrization of the vdW properties of the $[PF_6]^-$ and $[NO_3]^-$ atoms. This approach is in frame with the knowledge that the viscosity of the RTILs appears to be mostly dependent on the vdW interactions and H-bonding properties of the anion, as pointed out by Bonhôte et al.[45] The final parametrization for the anion species is presented in Table 2. We optimized our models to fit the experimental data as well as possible, in the following order of priority: cation and anion self-diffusion coefficients, shear viscosity, density, isothermal compressibility, and dihedral analysis. During the parametrization of a new liquid, it is easy to have a good agreement with experimental data on properties such as density. However, this might be accomplished with penalty on accuracy over other relevant properties such as the self-diffusion coefficient and the shear viscosity. For this reason, our models were primarily optimized against these two properties.

We also analyze other properties, namely, enthalpy of vaporization, radial/spatial distribution functions, and $\pi-\pi$ staking, to provide a more complete characterization of our model and for comparison with future experimental data.

Density. Tables 3 and 4 and Figure 2 present the temperature dependence of the density of both RTILs, as obtained experimentally[11,15] and by our simulations (averaged over 5-ns equilibrated trajectories). Our estimated densities are slightly underestimated for [BMIM][PF_6] (Figure 2A) and more accurate for [BMIM][NO_3] (Figure 2B), giving an overall good agreement with experimental data. Our results for [BMIM][PF_6] are better than those obtained with the united-atom model proposed by Shah et al.[6] and are as good as those obtained with other

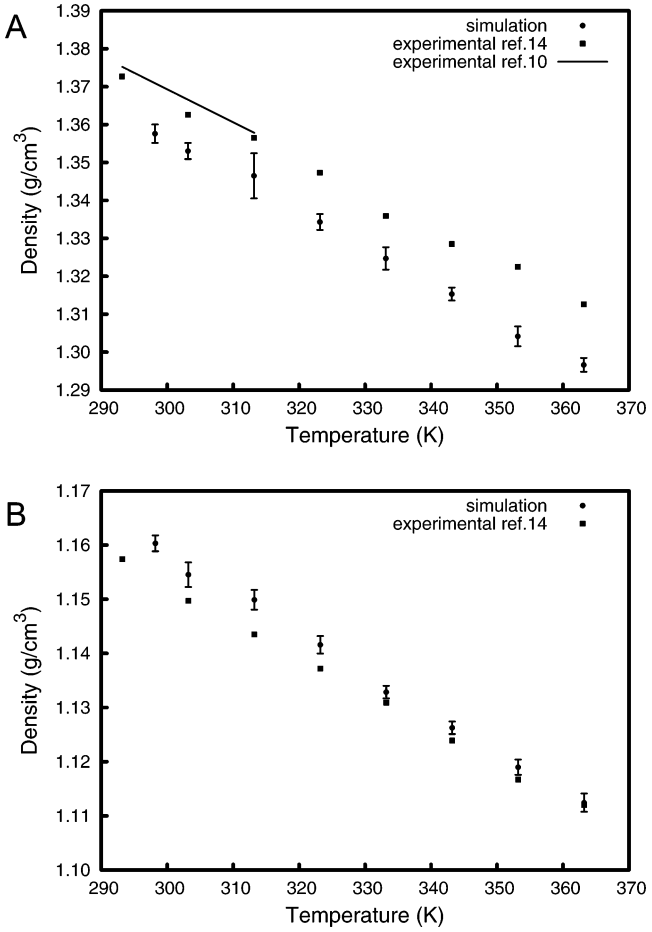

Figure 2. Experimental and simulation data concerning density of (A) [BMIM][PF_6] and (B) [BMIM][NO_3]. Closed squares correspond to experimental data reported by Seddon[15] with an experimental error of 0.0008 g/cm^3. The line in A corresponds to experimental results reported by Tokuda[11] as a linear equation fit. Closed circles correspond to simulation data. Error bars indicate two standard deviation units calculated with block averaging.

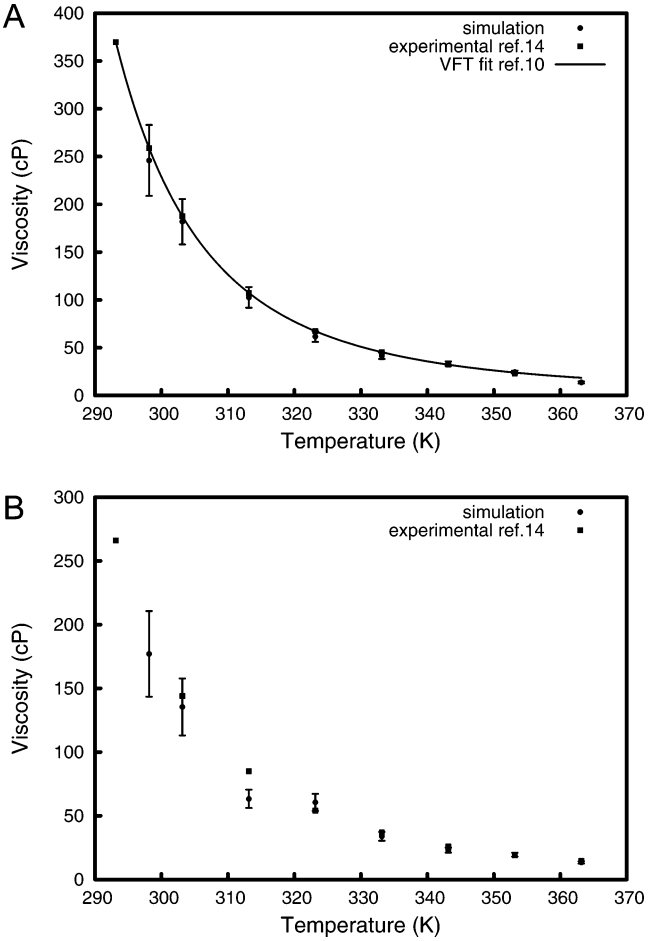

Figure 3. Experimental and simulation data concerning the viscosity of (A) [BMIM][PF_6] and (B) [BMIM][NO_3]. Closed squares are experimental data reported by Seddon[15] with an experimental error of 1% accuracy and 0.2% repeatability. The line in A corresponds to the experimental results reported by Tokuda[11] as a Vogel−Fulcher−Tamman (VFT) equation fit. Closed circles are simulation data. Errors in viscosity calculation from simulations are calculated using eq 25 from Hess.[56]

proposed all-atom models.[32,33,35] For [BMIM][PF_6] more accurate density estimations are obtained in the 298.15−323.15 K temperature range, whereas for [BMIM][NO_3] better estimations are obtained at higher temperatures.

Shear Viscosity. Shear viscosity is a useful property for the validation of a FF, given that in condensed phase it is governed by contributions from intermolecular interactions. Tables 3 and 4 and Figure 3 show the experimental and simulation data on this property. Shear viscosity measurements at different temperatures were reported for [BMIM][PF_6][11,15] and [BMIM][NO_3].[15,57] For both RTILs under study, the computed shear viscosity is slightly underestimated, being more accurate at higher temperatures. Globally, our model is able to reproduce, with good agreement, the experimental data and the general trend of the shear viscosity as a function of temperature.

Self-Diffusion. Recent reports of the self-diffusion coefficient data of [BMIM][PF_6] used the pulse-field gradient spin−echo NMR method.[11−13] This type of experimental data allows for an additional validation and characterization of the dynamical and transport properties of our [BMIM][PF_6] model. The self-diffusion coefficient is obtained easily from MD runs by the calculation of the mean square displacement (MSD) or velocity autocorrelation functions of the particles.[55] We obtained separate self-diffusion coefficients using MSD calculations of the cations and anions of our model RTILs and compared them with the experimental data available for [BMIM][PF_6]. Self-diffusion coefficients can be difficult to evaluate for this type of system because of the high rotational and translation motion correlation times expected for this model RTIL. As reported by Chitra and Yashonath,[58] the main conclusions of their study of estimating the error in the self-diffusion coefficient using MSD calculations are (1) the shorter the run length used for fitting, the greater will be the overestimation of self-diffusion coefficient and (2) fitting should avoid the initial and final regions. In the present work, we found that the self-diffusion coefficient calculation from a 5-ns-length MM/MD simulation fitted in the 2−4 ns interval should avoid the possibility of missing long-time correlation events and minimizes the overestimation of the self-diffusion coefficient. Our results (Tables 3 and 4, Figure 4) show that self-diffusion coefficients calculated from our model are accurate for the cation species and slightly lower for the anion, when compared with experimental data. Self-diffusion coefficients obtained from simulations have the same general temperature dependence trend found with experimental data. We consider that the diffusion properties of our model RTILs are acceptable when compared with the experimental data available.

Isothermal Compressibility. The isothermal compressibility was computed using the fluctuation of the volume of the system.[55] The isothermal compressibility for [BMIM][PF_6] at

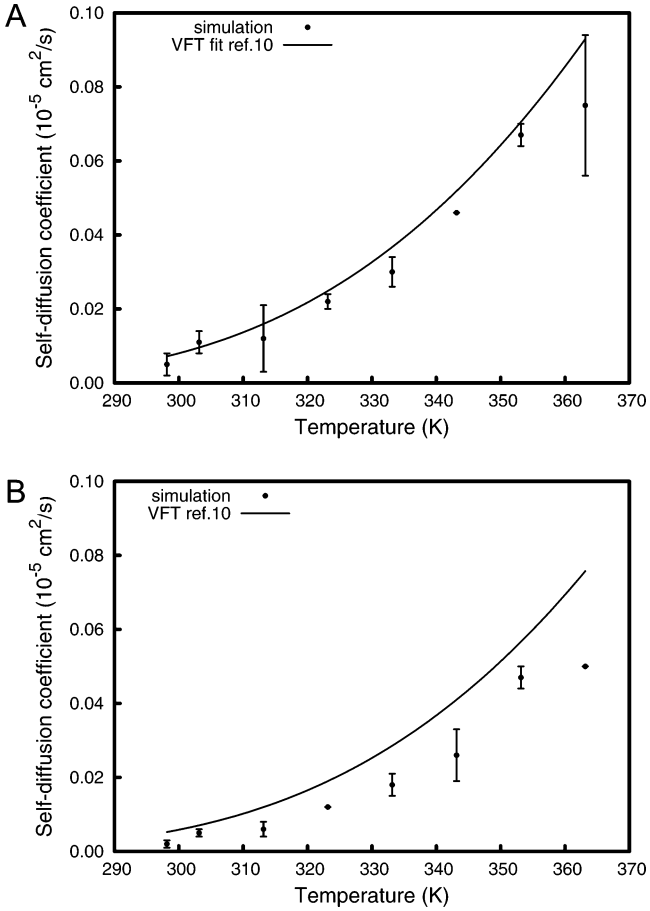

Figure 4. Experimental and simulation data of the self-diffusion coefficient of the (A) cation and (B) anion of [BMIM][PF_6]. The line corresponds to the experimental results reported by Tokuda[11] as a Vogel−Fulcher−Tamman (VFT) equation fit. Closed circles correspond to simulation data. The error is calculated as the difference of the self-diffusion coefficients obtained from fits over the two halves of the fit interval (see the text for details).

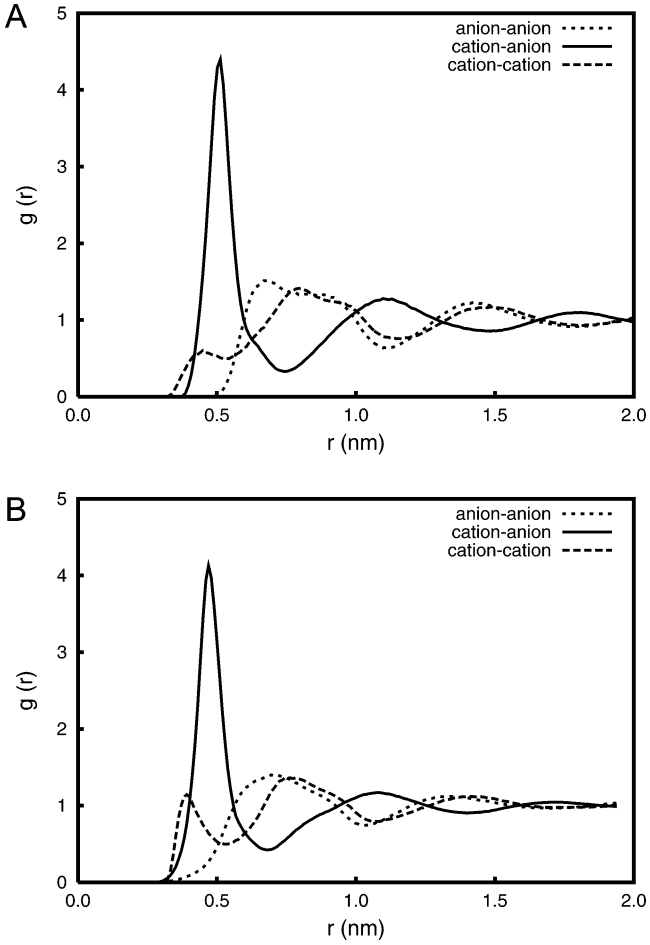

Figure 5. Radial distribution calculations of (A) [BMIM][PF_6] and (B) [BMIM][NO_3] at 298.15 K. Anion−anion, cation−cation, and cation−anion radial distributions are calculated using the geometric center of the [PF_6]$^-$ and [NO_3]$^-$ anions and the geometric center of the imidazole ring of the cation.

298.15 K is 31.12 × 10^{-6} bar^{-1}, similar to the experimental[20] value of 42.3 × 10^{-6} bar^{-1}, but not as good as predicted by the all-atom model proposed by Morrow and Maginn,[33] and slightly better than the prediction obtained with the united-atom model by Shah et al.[6]

Radial Distributions. A detailed picture of the liquid structure can be obtained from radial distribution functions, despite the fact that experimental data is not yet available for the systems studied here. The radial distributions of cations and anions for both RTILs at 298.15 K are shown in Figure 5. Although not necessarily relevant for validation, the [BMIM]-[PF_6] model generally agrees with other radial distributions for the same RTIL obtained by molecular simulations.[6,32,33] Note that, in the radial distributions calculations involving the cation molecule, only the atoms in the imidazole ring are considered. The cation−anion solvation peaks for [BMIM][PF_6] occur at 0.51, 1.12, and 1.78 nm, and for [BMIM][NO_3] at 0.47, 1.10, and 1.72 nm. By looking at the final part of the radial distribution, it can be seen that the [BMIM][PF_6] model is more structured than the [BMIM][NO_3] one. For both models, liquid ordering is found to persist beyond the 2 nm distance. At other temperatures within the studied range, the radial distribution functions for both RTILs remain very similar to the ones obtained at 298.15 K.

Anion Spatial Distribution. The spatial distribution probability of anions around cations in Figure 6 refines the molecular picture provided by the radial distribution functions of Figure 5. The spatial distribution probability indicates which regions around the cation are more populated by the anions. It is found that, as in other simulation studies of RTILs,[5,31,32,36] the anion distribution is found preferentially in the proximity of the aromatic hydrogens of the cation imidazole ring. The anion distribution exhibits larger amplitudes near the C2−H2 dipole and lower ones near the C4−H4 and C5−H5 dipoles, with densities slightly displaced to the left and right, respectively. Of notice is the extended distribution of [PF_6] anions in a position almost in plane with the imidazole ring (Figure 6A). The difference between [BMIM][NO_3] and [BMIM][PF_6] lies mostly in the distribution of anions around the C2−H2 dipole (Figure 6B). It seems that [NO_3]$^-$ anions prefer to be aligned with the C2−H2 dipole, when compared with the [PF_6]$^-$ anions.

π Interactions. Few studies have, so far, reported π-interaction analysis in RTILs. Downard et al.[42] reported the existence of $\pi-\pi$ stacking in long alkyl chain imidazolium chloride and [EMIM][CF_3SO_3]. In the case of [BMIM][Cl], X-ray diffraction studies found no evidence of ring $\pi-\pi$ stacking.[43] In our simulations, we analyzed the possible π interactions corresponding to the offset staked geometry (Figure 7) (see Waters[59] for a recent review). $\pi-\pi$ stacking geometries were searched from all the possible imidazole ring $\pi-\pi$ stacking pairs on each configuration from a 5-ns-length trajectory of [BMIM][PF_6] and [BMIM][NO_3] at 298.15 K. Analysis of $\pi-\pi$ stacking pairs was done in the same way as in Sony et al.[60] Only the $\pi-\pi$

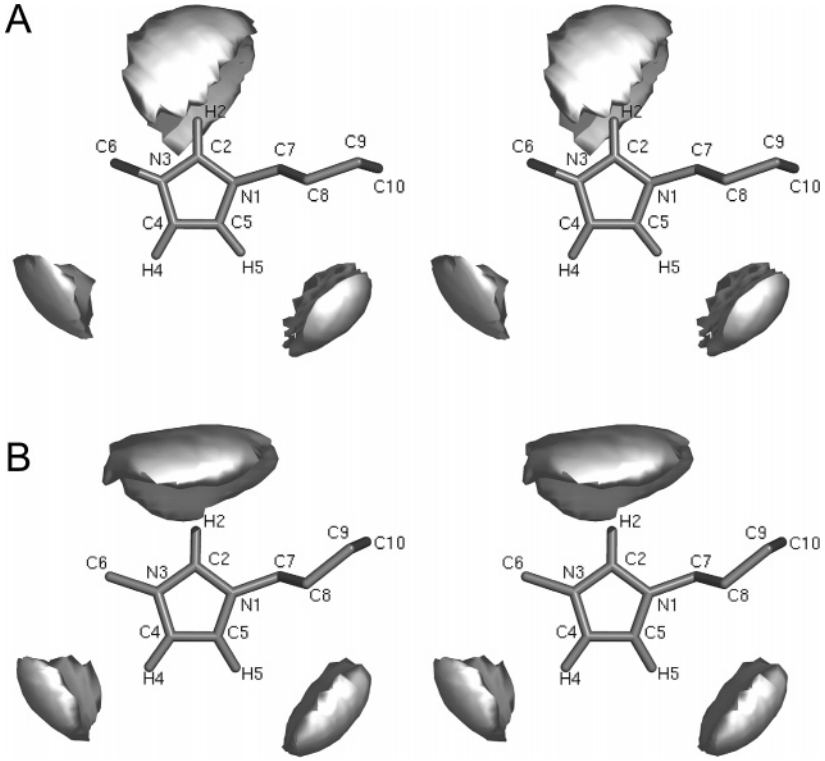

Figure 6. Spatial distribution probability density of cations around anions in (A) [BMIM][PF_6] and (B) [BMIM][NO_3] at 298.15 K. Cations at a maximum distance of 0.6 nm from the imidazole geometric center were selected. The contours enclose regions with a probability density above 0.0005.

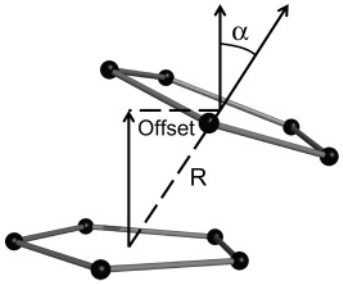

Figure 7. Schematic representation of a $\pi-\pi$ interaction between imidazole rings. The solid arrows represent the surface normals, *R* represents the distance between the two imidazole geometric centers, offset represents the ring offset, and α represents the angle between the two imidazole ring planes.

TABLE 5: Imidazole $\pi-\pi$ Interaction[a]

	R (Å)	offset (Å)	angle (deg)
ref 60	4.5 (5)	3 (1)	16 (26)
[BMIM][PF_6]	4.55 (0.003)	3.58 (0.007)	35.2 (0.12)
[BMIM][NO_3]	4.34 (0.002)	3.40 (0.005)	33.9 (0.09)

[a] $\pi-\pi$ interaction found in [BMIM][PF_6] and [BMIM][NO_3] at 298.15 K. See Figure 7 for details of the parameters used in the analysis. See Figure 8 for contour data of *R* vs angle.

interactions with a distance up to 5.2 Å between imidazole geometric centers were considered. Our RTIL models suggest the occurrence of a ring $\pi-\pi$ stacking, with ring geometric center distance (*R*), offset, and angle (Figure 7) within the experimental error of the imidazole−imidazole analysis reported by Sony et al.[60] (Table 5). However, the two RTILs under study are significantly different in all parameters. A detailed look of the normalized data of *R* versus angle distribution represented as contours on Figure 8 shows that the imidazole $\pi-\pi$ stacking configurations in [BMIM][NO_3] (Figure 8B) are highly concentrated in a particular geometry, whereas on [BMIM][PF_6] (Figure 8A) these configurations are more disperse (note that there is no 0.0020 contour level for this RTIL). It seems that the anion has an important role in determining the possibility of formation of this nonbonded interaction between cations.

Butyl Conformers. The coexistence of two butyl tail conformers in the liquid phase of [BMIM][Cl] is suggested to be one of the important reasons for the low melting points of RTILs.[44] The reported crystal polymorphism of [BMIM][Cl] due to gauche/trans conformations around the C_7-C_8 bond, also found in the liquid structure of [BMIM][Cl], [BMIM][Br] and [BMIM][I],[43,44] prompted us to analyze the configuration of this dihedral in our simulations. The potential energy function for the N1−C7−C8−C9 dihedral has three minima at ±180, −60, and +60, corresponding to one trans and two equivalent gauche conformers (Figure 9). The frequency distribution of this dihedral from our simulations at 298.15 K for both RTILs shows that all minima are populated, with a higher population for the trans than for the gauche conformers. Other parametrizations of [BMIM][PF_6] reported in the literature lack this feature.[35] This frequency distribution for both RTILs is equivalent, suggesting that in our model the two anion species do not interfere with the relative populations of trans/gauche cation conformers in the liquid phase.

Heat of Vaporization. The cohesion of the particles in the liquid phase can be measured by the enthalpy of vaporization (ΔH_{vap}) of the liquid. Our estimation of ΔH_{vap} is calculated as

$$\Delta H_{vap} = U_{pot}^{gas} - U_{pot}^{liq} + RT$$

and assumes that in the gas phase RTILs are formed by independent ion pairs. To have a more accurate description of the gas phase, 210 different ion pairs were sampled from the final conformation of the trajectories and simulated in vacuum for 500 ps. From these simulations, ion pair internal energies (U_{pot}^{gas}) were averaged. Our calculations show that ΔH_{vap} is very

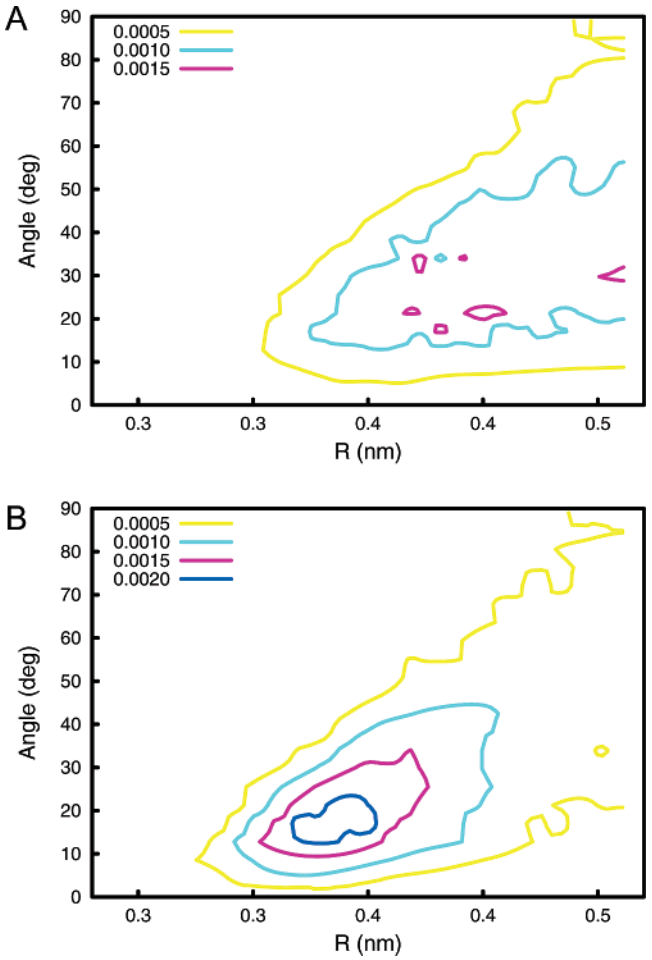

Figure 8. Contour data of R versus angle for the imidazole $\pi-\pi$ interaction for (A) [BMIM][PF_6] and (B) [BMIM][NO_3] and 298.15 K. See the text for analysis details. Note the absence of the 0.0020 contour level in [BMIM][PF_6].

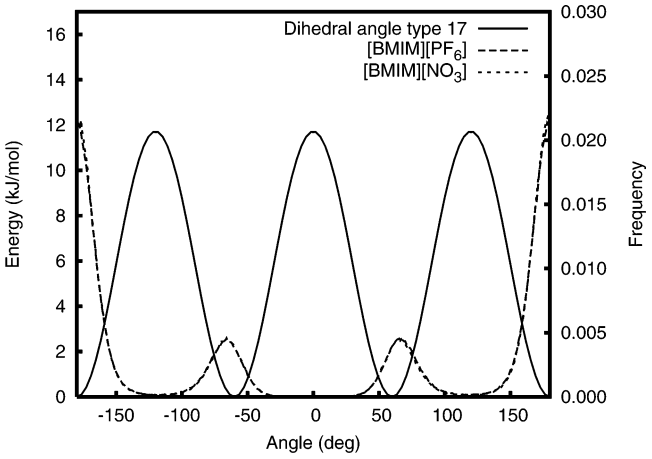

Figure 9. Torsion analysis of [BMIM]$^+$ N1−C7−C8−C9 dihedral angle (Figure 1). The solid line plots the GROMOS96 43A1[1] dihedral type 17 function applied to the dihedral angle in our molecular topology. Long and short dashed lines indicate the frequency histogram of this dihedral in our simulations at 298.15 K for [BMIM][PF_6] and [BMIM]-[NO_3], respectively.

high for both RTILs (Table 6) as previously suggested based on the low values measured for the vapor pressure.[61] It is also of notice that [BMIM][NO_3] RTIL has a higher ΔH_{vap} than [BMIM][PF_6].

TABLE 6: Computed Vaporization Enthalpies (ΔH_{vap})

	ΔH_{vap} (kJ/mol)	
temp (K)	[BMIM][PF_6]	[BMIM][NO_3]
298.15	123.3	130.2
303.15	122.4	128.5
313.15	119.6	126.6
323.15	117.5	123.6
333.15	115.2	121.0
343.15	112.9	118.8
353.15	110.5	117.0
363.15	109.0	114.7

Concluding Remarks

Using the available experimental data for the liquid phase of [BMIM][PF_6] and [BMIM][NO_3], we developed a united-atom model for these two liquids in the context of the GROMOS96 43A1 FF.[1] This is the first study of RTIL parametrization for this biomolecular FF. The computed densities, self-diffusion coefficients, and viscosities are in good agreement with the experimental data. Isothermal compressibility is shown to be in reasonable agreement with experiment also. The radial and spatial distribution probabilities of cations and anions revealed the spatial positioning of the anions around the imidazole ring modeled by our parametrization, and possibly how it occurs in the real solution. A recent analysis of π interactions of nitrogen-containing heterocyclic systems[60] provides a good comparison with our simulations, suggesting the existence of this type of nonbonded interaction between cations for the two models under study, and differences between them. Analysis of the configurations of trans/gauche conformers of the butyl tail show that our united-atom model and the simulation times of the study presented here are able to sample these two cation configurations. Enthalpies of vaporization are calculated for the range of temperature analyzed, and are found to be quite high, consistent with the low vapor pressure of these liquids. These quantities are presented here for further reference, given that there are no experimental measurements of these values. The two RTILs reproduce important physical aspects of the liquid phase and, given their development within the framework of a biomolecular force field, we are confident that they can be used in heterogeneous systems, such as liquid mixtures and as solvents of proteins.

Acknowledgment. We acknowledge helpful discussions with Dr. Luís Paulo Rebelo, and the financial support from Fundação para a Ciência e a Tecnologia, Portugal, through grants PRAXIS/P/BIO/14314/1998, POCTI/BIO/57193/04, and SFRH/BD/10611/2002.

References and Notes

(1) Scott, W. R. P.; Hunenberger, P. H.; Tironi, I. G.; Mark, A. E.; Billeter, S. R.; Fennen, J.; Torda, A. E.; Huber, T.; Kruger, P.; van Gunsteren, W. F. *J. Phys. Chem. A* **1999**, *103*, 3596.

(2) Cornell, W. D.; Cieplak, P.; Bayly, C. I.; Gould, I. R.; Merz, K. M.; Ferguson, D. M.; Spellmeyer, D. C.; Fox, T.; Caldwell, J. W.; Kollman, P. A. *J. Am. Chem. Soc.* **1996**, *118*, 2309.

(3) Jorgensen, W. L.; Maxwell, D. S.; TiradoRives, J. *J. Am. Chem. Soc.* **1996**, *118*, 11225.

(4) MacKerell, A. D.; Bashford, D.; Bellott, M.; Dunbrack, R. L.; Evanseck, J. D.; Field, M. J.; Fischer, S.; Gao, J.; Guo, H.; Ha, S.; Joseph-McCarthy, D.; Kuchnir, L.; Kuczera, K.; Lau, F. T. K.; Mattos, C.; Michnick, S.; Ngo, T.; Nguyen, D. T.; Prodhom, B.; Reiher, W. E.; Roux, B.; Schlenkrich, M.; Smith, J. C.; Stote, R.; Straub, J.; Watanabe, M.; Wiorkiewicz-Kuczera, J.; Yin, D.; Karplus, M. *J. Phys. Chem. B* **1998**, *102*, 3586.

(5) Hanke, C. G.; Price, S. L.; Lynden-Bell, R. M. *Mol. Phys.* **2001**, *99*, 801.

(6) Shah, J. K.; Brennecke, J. F.; Maginn, E. J. *Green Chem.* **2002**, *4*, 112.
(7) Liu, Z. P.; Wu, X. P.; Wang, W. C. *Phys. Chem. Chem. Phys.* **2006**, *8*, 1096.
(8) Wilkes, J. S. *J. Mol. Catal. A* **2004**, *214*, 11.
(9) Dupont, J.; de Souza, R. F.; Suarez, P. A. Z. *Chem. Rev.* **2002**, *102*, 3667.
(10) Olivier-Bourbigou, H.; Magna, L. *J. Mol. Catal. A* **2002**, *182*, 419.
(11) Tokuda, H.; Hayamizu, K.; Ishii, K.; Abu Bin Hasan Susan, M.; Watanabe, M. *J. Phys. Chem. B* **2004**, *108*, 16593.
(12) Umecky, T.; Kanakubo, M.; Ikushima, Y. *Fluid Phase Equilib.* **2005**, *228*, 329.
(13) Umecky, T.; Kanakubo, M.; Ikushima, Y. *J. Mol. Liq.* **2005**, *119*, 77.
(14) Baker, S. N.; Baker, G. A.; Kane, M. A.; Bright, F. V. *J. Phys. Chem. B* **2001**, *105*, 9663.
(15) Seddon, K. R.; Stark, A.; Torres, M. J. *Clean Solvents* **2002**, *819*, 34.
(16) Carda-Broch, S.; Berthod, A.; Armstrong, D. W. *Anal. Bioanal. Chem.* **2003**, *375*, 191.
(17) Koel, M. *Proc. Est. Acad. Sci., Chem.* **2000**, *49*, 145.
(18) Dzyuba, S. V.; Bartsch, R. A. *ChemPhysChem* **2002**, *3*, 161.
(19) Huddleston, J. G.; Visser, A. E.; Reichert, W. M.; Willauer, H. D.; Broker, G. A.; Rogers, R. D. *Green Chem.* **2001**, *3*, 156.
(20) Gu, Z. Y.; Brennecke, J. F. *J. Chem. Eng. Data* **2002**, *47*, 339.
(21) Fredlake, C. P.; Crosthwaite, J. M.; Hert, D. G.; Aki, S. N. V. K.; Brennecke, J. F. *J. Chem. Eng. Data* **2004**, *49*, 954.
(22) Kabo, G. J.; Blokhin, A. V.; Paulechka, Y. U.; Kabo, A. G.; Shymanovich, M. P.; Magee, J. W. *J. Chem. Eng. Data* **2004**, *49*, 453.
(23) Headley, A. D.; Jackson, N. M. *J. Phys. Org. Chem.* **2002**, *15*, 52.
(24) Antony, J. H.; Mertens, D.; Dolle, A.; Wasserscheid, P.; Carper, W. R. *ChemPhysChem* **2003**, *4*, 588.
(25) Chakrabarty, D.; Harza, P.; Chakraborty, A.; Seth, D.; Sarkar, N. *Chem. Phys. Lett.* **2003**, *381*, 697.
(26) Karmakar, R.; Samanta, A. *J. Phys. Chem. A* **2002**, *106*, 4447.
(27) Ingram, J. A.; Moog, R. S.; Ito, N.; Biswas, R.; Maroncelli, M. *J. Phys. Chem. B* **2003**, *107*, 5926.
(28) Hardacre, C.; McMath, S. E. J.; Nieuwenhuyzen, M.; Bowron, D. T.; Soper, A. K. *J. Phys.: Condens. Matter* **2003**, *15*, S159.
(29) Triolo, A.; Russina, O.; Arrighi, V.; Juranyi, F.; Janssen, S.; Gordon, C. M. *J. Chem. Phys.* **2003**, *119*, 8549.
(30) Fuller, J.; Carlin, R. T.; Delong, H. C.; Haworth, D. *J. Chem. Soc., Chem. Commun.* **1994**, 299.
(31) Del Popolo, M. G.; Lynden-Bell, R. M.; Kohanoff, J. *J. Phys. Chem. B* **2005**, *109*, 5895.
(32) Liu, Z. P.; Huang, S. P.; Wang, W. C. *J. Phys. Chem. B* **2004**, *108*, 12978.
(33) Morrow, T. I.; Maginn, E. J. *J. Phys. Chem. B* **2002**, *106*, 12807.
(34) de Andrade, J.; Boes, E. S.; Stassen, H. *J. Phys. Chem. B* **2002**, *106*, 3546.
(35) Margulis, C. J.; Stern, H. A.; Berne, B. J. *J. Phys. Chem. B* **2002**, *106*, 12017.
(36) Del Popolo, M. G.; Voth, G. A. *J. Phys. Chem. B* **2004**, *108*, 1744.
(37) Yan, T. Y.; Burnham, C. J.; Del Popolo, M. G.; Voth, G. A. *J. Phys. Chem. B* **2004**, *108*, 11877.
(38) Oostenbrink, C.; Villa, A.; Mark, A. E.; Van Gunsteren, W. F. *J. Comput. Chem.* **2004**, *25*, 1656.
(39) Bayly, C. I.; Cieplak, P.; Cornell, W. D.; Kollman, P. A. *J. Phys. Chem.* **1993**, *97*, 10269.
(40) Frisch, M. J.; Trucks, G. W.; Schlegel, H. B.; Scuseria, G. E.; Robb, M. A.; Cheeseman, J. R.; Zakrzewski, V. G.; Montgomery, J. A., Jr.; Stratmann, R. E.; Burant, J. C.; Dapprich, S.; Millam, J. M.; Daniels, A. D.; Kudin, K. N.; Strain, M. C.; Farkas, O.; Tomasi, J.; Barone, V.; Cossi, M.; Cammi, R.; Mennucci, B.; Pomelli, C.; Adamo, C.; Clifford, S.; Ochterski, J.; Petersson, G. A.; Ayala, P. Y.; Cui, Q.; Morokuma, K.; Malick, D. K.; Rabuck, A. D.; Raghavachari, K.; Foresman, J. B.; Cioslowski, J.; Ortiz, J. V.; Stefanov, B. B.; Liu, G.; Liashenko, A.; Piskorz, P.; Komaromi, I.; Gomperts, R.; Martin, R. L.; Fox, D. J.; Keith, T.; Al-Laham, M. A.; Peng, C. Y.; Nanayakkara, A.; Gonzalez, C.; Challacombe, M.; Gill, P. M. W.; Johnson, B. G.; Chen, W.; Wong, M. W.; Andres, J. L.; Head-Gordon, M.; Replogle, E. S.; Pople, J. A. *Gaussian 98*, revision A.7; Gaussian, Inc.: Pittsburgh, PA, 1998.
(41) van Gunsteren, W. F.; Billeter, S. R.; Eising, A. A.; Hünenberger, P. H.; Kruger, P.; Mark, A. E.; Scott, W. R. P.; Tironi, I. G. *Biomolecular Simulation: The GROMOS96 Manual and User Guide*; Zurich, Groninger, 1996.
(42) Downard, A.; Earle, M. J.; Hardacre, C.; McMath, S. E. J.; Nieuwenhuyzen, M.; Teat, S. J. *Chem. Mater.* **2004**, *16*, 43.
(43) Saha, S.; Hayashi, S.; Kobayashi, A.; Hamaguchi, H. *Chem. Lett.* **2003**, *32*, 740.
(44) Katayanagi, H.; Hayashi, S.; Hamaguchi, H. O.; Nishikawa, K. *Chem. Phys. Lett.* **2004**, *392*, 460.
(45) Bonhote, P.; Dias, A. P.; Papageorgiou, N.; Kalyanasundaram, K.; Gratzel, M. *Inorg. Chem.* **1996**, *35*, 1168.
(46) Hardacre, C.; Holbrey, J. D.; McMath, S. E. J.; Bowron, D. T.; Soper, A. K. *J. Chem. Phys.* **2003**, *118*, 273.
(47) Dupont, J. *J. Braz. Chem. Soc.* **2004**, *15*, 341.
(48) Berendsen, H. J. C.; van der Spoel, D.; van Drunen, R. *Comput. Phys. Commun.* **1995**, *91*, 43.
(49) Lindahl, E.; Hess, B.; van der Spoel, D. *J. Mol. Model.* **2001**, *7*, 306.
(50) Hess, B.; Bekker, H.; Berendsen, H. J. C.; Fraaije, J. G. E. M. *J. Comput. Chem.* **1997**, *18*, 1463.
(51) Essmann, U.; Perera, L.; Berkowitz, M. L.; Darden, T.; Lee, H.; Pedersen, L. G. *J. Chem. Phys.* **1995**, *103*, 8577.
(52) Darden, T.; York, D.; Pedersen, L. *J. Chem. Phys.* **1993**, *98*, 10089.
(53) Berendsen, H. J. C.; Postma, J. P. M.; van Gunsteren, W. F.; Dinola, A.; Haak, J. R. *J. Chem. Phys.* **1984**, *81*, 3684.
(54) Ciccotti, G.; Jacucci, G.; McDonald, I. R. *J. Stat. Phys.* **1979**, *21*, 1.
(55) Allen, M. P.; Tildesley, D. J. *Computer Simulation of Liquids*; Oxford University Press: Oxford, 1997.
(56) Hess, B. *J. Chem. Phys.* **2002**, *116*, 209.
(57) Seddon, K. R.; Stark, A.; Torres, M. J. *Pure Appl. Chem.* **2000**, *72*, 2275.
(58) Chitra, R.; Yashonath, S. *J. Phys. Chem. B* **1997**, *101*, 5437.
(59) Waters, M. L. *Curr. Opin. Chem. Biol.* **2002**, *6*, 736.
(60) Sony, S. M. M.; Ponnuswamy, M. N. *Cryst. Growth Des.* **2006**, *6*, 736.
(61) Paulechka, Y. U.; Kabo, G. J.; Blokhin, A. V.; Vydrov, O. A.; Magee, J. W.; Frenkel, M. *J. Chem. Eng. Data* **2003**, *48*, 457.